



This discussion paper is/has been under review for the journal Earth System Dynamics (ESD). Please refer to the corresponding final paper in ESD if available.

Inter-hemispheric asymmetry in the sea-ice response to volcanic forcing simulated by MPI-ESM (COSMOS-Mill)

D. Zanchettin¹, O. Bothe², C. Timmreck¹, J. Bader¹, A. Beitsch¹, H.-F. Graf³,
D. Notz¹, and J. H. Jungclaus¹

¹Max Planck Institute for Meteorology, Bundesstr. 53, 20146 Hamburg, Germany

²Leibniz Institute of Atmospheric Physics at the University of Rostock, Kühlungsborn, Germany

³University of Cambridge, Centre for Atmospheric Science, Downing Place, Cambridge, CB2 3EN, UK

Received: 7 January 2014 – Accepted: 22 January 2014 – Published: 3 February 2014

Correspondence to: D. Zanchettin (davide.zanchettin@mpimet.mpg.de)

Published by Copernicus Publications on behalf of the European Geosciences Union.

Inter-hemispheric asymmetry in the sea-ice response to volcanic forcing

D. Zanchettin et al.

Title Page

Abstract

Introduction

Conclusions

References

Tables

Figures



Back

Close

Full Screen / Esc

Printer-friendly Version

Interactive Discussion



Abstract

The decadal evolution of Arctic and Antarctic sea ice following strong volcanic eruptions is investigated in four climate simulation ensembles performed with the COSMOS-Mill version of the Max Planck Institute-Earth System Model. The ensembles differ in the magnitude of the imposed volcanic perturbations, with sizes representative of historical tropical eruptions (1991 Pinatubo and 1815 Tambora) and of tropical and extra-tropical “supervolcano” eruptions. A post-eruption Arctic sea-ice expansion is robustly detected in all ensembles, while Antarctic sea ice responds only to “supervolcano” eruptions, undergoing an initial short-lived expansion and a subsequent prolonged contraction phase. Strong volcanic forcing therefore emerges as a potential source of inter-hemispheric interannual-to-decadal climate variability, although the inter-hemispheric signature is weak in the case of historical-size eruptions. The post-eruption inter-hemispheric decadal asymmetry in sea ice is interpreted as a consequence mainly of different exposure of Arctic and Antarctic regional climates to induced meridional heat transport changes and of dominating local feedbacks that set in within the Antarctic region. “Supervolcano” experiments help clarifying differences in simulated hemispheric internal dynamics related to imposed negative net radiative imbalances, including the relative importance of the thermal and dynamical components of the sea-ice response. “Supervolcano” experiments could therefore serve the assessment of climate models’ behavior under strong external forcing conditions and, consequently, favor advancements in our understanding of simulated sea-ice dynamics.

1 Introduction

Polar regional climates are in the focus of Earth system investigations owing to their strong sensitivity to external forcing and associated implications for the global climate. The so-called “polar amplification” of climate signals is mainly a consequence of positive feedbacks involving snow cover and sea ice, and it emerges more robustly in the

ESDD

5, 121–168, 2014

Inter-hemispheric asymmetry in the sea-ice response to volcanic forcing

D. Zanchettin et al.

Title Page

Abstract

Introduction

Conclusions

References

Tables

Figures

⏪

⏩

◀

▶

Back

Close

Full Screen / Esc

Printer-friendly Version

Interactive Discussion



Inter-hemispheric asymmetry in the sea-ice response to volcanic forcing

D. Zanchettin et al.

Title Page

Abstract

Introduction

Conclusions

References

Tables

Figures



Back

Close

Full Screen / Esc

Printer-friendly Version

Interactive Discussion

Northern than in the Southern Hemisphere (e.g. Parkinson, 2004). The different behavior of Arctic and Antarctic sea ice is largely explained by the different geographical characteristics of the two polar regions: the semi-enclosed Arctic Ocean limits sea-ice mobility and favors sea-ice thickening and persistence while making Arctic sea ice strongly susceptible to changes in the Atlantic Ocean's northward heat transport and to anomalous atmospheric heat inflows from the surrounding landmasses. Antarctic sea-ice, by contrast, forms around the Antarctica landmass in the open Southern Ocean, its northern boundary being set by the circumpolar system of southern mid-latitude westerly winds and ocean currents. This system makes Antarctic sea ice strongly subject to equatorward drifting and melting – which explains its weak persistence – while limiting its exposure to global changes and associated anomalous atmospheric and oceanic meridional heat flows (e.g. Zhang, 2007, 2014). Still, important processes driving this critical component of the Earth system remain unresolved and, hence, not robustly simulated by coupled global circulation models and Earth System Models (e.g. Maksym et al., 2012; Turner et al., 2013). Aiming at a better understanding of simulated global sea-ice behavior and of its sensitivity to external forcing, this study investigates the decadal evolution of Arctic and Antarctic sea ice in a set of idealized volcanically-forced experiments conducted with a full-complexity Earth System Model. Focus is on inter-hemispheric differences in the sea-ice response.

Observations covering the past three decades point to an inter-hemispheric asymmetry in recent sea-ice cover evolution: while the decline in Arctic total sea-ice cover is among the most notable features related to present climate change (e.g. Notz and Marotzke, 2012; Stroeve et al., 2012; Wang and Overland, 2012), the Antarctic total sea-ice cover has remained steady, or even increased slightly (Stammerjohn et al., 2012; Massonnet et al., 2013). Despite generally improved representations of observed sea-ice climatology and evolution (Stroeve et al., 2012), reproduction of the observed Arctic/Antarctic sea-ice dichotomy remains a challenge for state-of-the-art coupled climate models (Maksym et al., 2012; Turner et al., 2013). Internal climate variability spreads simulated Arctic (Stroeve et al., 2012) as well as Antarctic (Polvani

Inter-hemispheric asymmetry in the sea-ice response to volcanic forcing

D. Zanchettin et al.

Title Page

Abstract

Introduction

Conclusions

References

Tables

Figures

⏪

⏩

◀

▶

Back

Close

Full Screen / Esc

Printer-friendly Version

Interactive Discussion

vertical levels with the highest one (i.e. the model top) set at 10 hPa. The model's low top restrict the description of stratospheric and coupled stratosphere-troposphere dynamics (e.g. Omrani et al., 2014), which may affect the dynamical atmospheric response to volcanic forcing (e.g. Charlton-Perez et al., 2013). MPIOM is run in its standard configuration GR30L40, corresponding to a horizontal grid-spacing of about 3.0° and 40 vertical levels. It embeds a dynamic-thermodynamic Hibler-type sea-ice model. A detailed description of the treatment of sub grid-scale mixing and of the sea-ice dynamics and thermodynamics implemented in MPIOM is provided by Marsland et al. (2003). Modules for terrestrial biosphere (JSBACH, see: Raddatz et al., 2007) and for ocean biogeochemistry (HAMOCC, see: Wetzel et al., 2005) allow for an interactive representation of the carbon cycle.

Four simulation ensembles are considered describing the climatic effects of idealized volcanic perturbations of different magnitude, up to “supervolcano”-size eruptions. The four ensembles consist of (i) ten simulations forced by a 1991 Pinatubo-like tropical eruption, (ii) ten simulations forced by a 1815 Tambora-like tropical eruption, (iii) five simulations forced by a Young Toba Tuff (Toba)-like eruption, i.e. a tropical eruption with 100-times the emission strength of the Pinatubo eruption, and (iv) ten simulations forced by a Yellowstone-like eruption (i.e. same as Toba, but located in the Northern Hemisphere's mid-latitudes). In the following, we refer to the ensembles avoiding the volcanoes' specific names to highlight their idealized character. We thereafter refer to the Pinatubo and Tambora simulations/eruptions as “historical” (namely HIST1 and HIST2, respectively), since these eruptions are representative of the magnitude of volcanic eruptions that occurred during the last millennium. The Toba and Yellowstone “supervolcano” ensembles are referred to as SUPER1 and SUPER2, respectively. HIST2 corresponds to the VO2 ensemble in Zanchettin et al. (2013). SUPER1 entails the simulations used in Timmreck et al. (2010, 2012). SUPER2 simulations are those described in Segschneider et al. (2012). Each ensemble consists of simulations differing only in their initial climate states, which are sampled from a multi-millennial pre-industrial control simulation (as used in Timmreck et al., 2010; and Zanchettin

eruption employing the same volcanic forcing input as the HIST2 ensemble are compatible with estimates from observations and reconstructions (Zanchettin et al., 2013).

Responses are diagnosed through analysis of ensemble-averages. For time series, we use deseasonalized and then low-pass filtered values. Seasonality is computed based on control-run data and then subtracted from all data. Filtering consists of 3 month centered running-mean for atmospheric variables, and 13 month centered running-mean for oceanic and sea-ice variables, unless specified otherwise. Anomalies are evaluated as deviations from the pre-eruption climatology, defined as the mean climate state during the ten years/winters/summers preceding the eruption. Post-eruption years are progressively numbered starting from the year of the eruption, which is defined as year 0.

A Monte-Carlo approach is used to estimate the statistical significance of the forced signals (e.g. Graf and Zanchettin, 2012). Specifically, the ensemble-average signals obtained from an ensemble of n forced simulations are compared with a large set of analog ensemble-average signals (here 500) obtained by randomly sampling n years along the whole length of the control run. The empirical distribution yielded by these analog ensemble-average signals describes probabilistically the range explicable by internal variability alone, which we also interpret as the confidence level of corresponding signals in the forced ensembles having occurred by chance. We consider as reference the 98 % range (i.e. 1st–99th percentile band) of such distribution in order to have a conservative estimate of internal variability signals. Since the procedure is only based on the random selection of years, the autocorrelation is preserved in the estimation of the significance.

Total sea-ice area in the Arctic and in the Antarctic is calculated as the areal sum of sea ice covering the ocean in the Northern and Southern Hemispheres, respectively. Analogously, total sea-ice volume is defined as the sum of local (i.e. grid-point) products of grid-cell area and grid-cell-average sea-ice thickness. The sea-ice edge is defined as the line denoting the sea-ice extent margin, i.e. the area enclosing sea-ice

Inter-hemispheric asymmetry in the sea-ice response to volcanic forcing

D. Zanchettin et al.

Title Page

Abstract

Introduction

Conclusions

References

Tables

Figures



Back

Close

Full Screen / Esc

Printer-friendly Version

Interactive Discussion



concentrations exceeding the 0.15 threshold (in the range [0 : 1], where 0 indicates no sea ice in the grid-cell and 1 indicates sea ice fully covering the grid-cell).

Meridional ocean heat transports HT are calculated at 60° N and 60° S as in Zanchettin et al. (2012) based on the equation: $HT = \sum_z \sum_x v T c_p \rho dx dz$, where v is the meridional velocity component, T is temperature, c_p is specific heat capacity at constant pressure, ρ is density, and dz and dx represent, respectively, the integrals along depths and longitudes. The zonal mean component of the total meridional ocean heat transports is considered to be associated with the overturning transport; the residual component is considered to describe the gyre contribution to the total meridional ocean heat transport. Accordingly, deviations of v and T from the respective zonal mean values are used in the above mentioned equation for the calculation of the gyre contribution to HT.

The meridional atmospheric energy transport around 60° N and 60° S are defined, following Keith (1995), as the zonal integral at, respectively, 61.23° N and 61.23° S of the convergence of the atmospheric energy transport vector F_A , which can be written for latitude λ as:

$$F_\lambda = \int_\lambda -\nabla * F_A dx = \int_\lambda -\nabla * \frac{1}{g} \int_0^{p_s} (c_p T + \Phi + Lq + k) \mathbf{v} dp dx \quad (1)$$

where dp and dx represent, respectively, the integral along pressure levels and longitudes, $c_p T + \Phi$ represents the dry static energy, with the specific heat of the atmosphere at constant pressure c_p , temperature T , and geopotential Φ . The moist static energy is depicted by $c_p T + \Phi + Lq$, with latent heat of evaporation/condensation L , and specific humidity q . The horizontal wind vector is represented by \mathbf{v} . As kinetic energy k is typically a small component of the energy budget, it is ignored in the following. The small latitudinal difference between atmospheric and oceanic heat transport calculations is of negligible concern, since we do not aim to close the energy budget for the two regions.

Inter-hemispheric asymmetry in the sea-ice response to volcanic forcing

D. Zanchettin et al.

Title Page

Abstract

Introduction

Conclusions

References

Tables

Figures

◀

▶

◀

▶

Back

Close

Full Screen / Esc

Printer-friendly Version

Interactive Discussion

3 Results

3.1 Imposed forcing and global/hemispheric responses

The imposed forcing is very well constrained within each of the four ensembles (Fig. 1). Estimates based on top-of-atmosphere radiative anomalies for individual ensembles are consistent with previously reported ones (Timmreck et al., 2010; Segschneider et al., 2012; Zanchettin et al., 2013); we therefore describe only major features and inter-ensemble differences. Especially during the first three post-eruption years, ensemble standard errors are barely distinguishable from the corresponding ensemble-average values. Peak negative anomalies in the global top-of-atmosphere net radiative flux range between $\sim -3 \text{ W m}^{-2}$ for HIST1 and $\sim -27 \text{ W m}^{-2}$ for SUPER2 (Fig. 1c). SUPER2 leads to a slightly stronger forcing than SUPER1 in the net radiative flux estimate (Fig. 1c). This highlights the dependence of the net forcing on the shape of post-eruption evolutions of the shortwave and longwave radiation flux anomalies, since these have otherwise similar peak values in the two ensembles (Fig. 1a and b). The evolution of radiative fluxes is directly linked to the evolution of the volcanic aerosol mass, which builds up slower during the first post-eruption months in SUPER2 compared to SUPER1 (not shown). This seems to be the key to understanding the differences between the two “supervolcano” ensembles and the distinguishing traits of the former. The positive net flux anomaly around lags of 42 to 78 months is mainly a consequence of the ocean releasing less latent heat to the atmosphere (Timmreck et al., 2010; Zanchettin et al., 2013).

On the global scale, the four ensembles depict significant post-eruption drops in surface (2 m) air temperature and precipitation (Fig. 2a and b). Cold temperature anomalies consistently peak in the boreal summer-autumn of year 1, i.e. slightly after the peak in the forcing (compare with Fig. 1c), with larger ensemble spread for the historical eruptions (note, SUPER1 consists of only five simulations). HIST1 displays a temporary initial recovery of the temperature signal to within the internal variability range in year 2, when typically a warm ENSO event sets in. The ensemble-mean simulated maximum

Inter-hemispheric asymmetry in the sea-ice response to volcanic forcing

D. Zanchettin et al.

Title Page

Abstract

Introduction

Conclusions

References

Tables

Figures



Back

Close

Full Screen / Esc

Printer-friendly Version

Interactive Discussion



**Inter-hemispheric
asymmetry in the
sea-ice response to
volcanic forcing**D. Zanchettin et al.

[Title Page](#)[Abstract](#)[Introduction](#)[Conclusions](#)[References](#)[Tables](#)[Figures](#)[Back](#)[Close](#)[Full Screen / Esc](#)[Printer-friendly Version](#)[Interactive Discussion](#)

cooling for HIST1 matches the observed maximum cooling of 0.4 K estimated for the Pinatubo by Thompson et al. (2009). Annual oscillations in the post-eruption anomalous temperature evolution in the “supervolcano” ensembles indicate a seasonal differentiation of the response, with boreal winter semesters being comparatively colder than summer ones from year 2 onwards. The global temperature responses differ appreciably between SUPER1 and SUPER2. Inter-ensemble differences in global precipitation regard the timing of the post-eruption fluctuation, delayed in the case of SUPER2 compared to SUPER1, rather than the shape of the post-eruption fluctuation and its peak value. Post-eruption anomalies of hemispheric-average surface air temperature (Fig. 2c and d) further highlight the differences between historical and “supervolcano” eruptions. For the two historical eruptions, inter-hemispheric differences are small and remain mostly confined within the internal variability range after the first two post-eruption years (Fig. 2d). For the “supervolcano” ensembles, inter-hemispheric differences are large and remarkably independent of the location of the eruption (Fig. 2d): the Northern Hemisphere undergoes a much stronger and longer lasting cooling compared to the historical ensembles (Fig. 2c), with a more pronounced seasonal character than the Southern Hemisphere (compare Fig. 2d). As a consequence, in both “supervolcano” ensembles the anomalous hemispheric temperature evolutions deviate considerably from the global estimate.

Overall, we diagnose qualitatively similar features in the different ensembles that point to an amplification of the forced global signals with increased magnitude of the eruption. “Supervolcano” simulations feature a high signal-to-noise ratio, and even the 5-member SUPER1 ensemble is suitable for robust global/hemispheric-scale inferences. Inter-hemispheric differences are apparent in the surface air temperature responses to “supervolcano” but not historical-size eruptions, suggesting that substantially different dynamical responses may characterize the different eruption sizes.

3.2 Sea-ice response

The post-eruption anomalies of Arctic and Antarctic sea-ice area and volume depict major inter-hemispheric differences in the sea-ice responses to both historical and “supervolcano” eruptions (Fig. 3). In the Arctic, the total sea ice expands for all eruptions (Fig. 3a and c). The post-eruption positive anomalies of total Arctic sea-ice area and volume are of comparable magnitude for the two historical eruptions, but their timing differs. Total Arctic sea-ice area and volume anomalies are about one order of magnitude larger in the “supervolcano” ensembles compared to historical ones. In both ensembles, total sea-ice area and volume entail a sharp increase in simulation years 1 and 2, which is followed by a decadal-scale progressive dampening of the anomaly. The larger anomalies in SUPER2 compared to SUPER1 are likely thermally driven: the volcanic cloud produced by the extra-tropical Yellowstone-like eruption is more confined to the Northern Hemisphere and produces a stronger radiative effect there, i.e. stronger cooling (Fig. 2d). The system fully reverts back to within the internal variability range in about 2–2.5 decades.

Significant post-eruption anomalies of Antarctic total sea-ice area and volume (Fig. 3b and d) are only detected in the “supervolcano” ensembles. In these ensembles and especially concerning the total sea-ice volume, Antarctic sea-ice anomalies are much smaller than their Arctic counterparts (compare Fig. 3c and d). This is true for both the actual anomalies and their values relative to the pre-eruption climatology (which is reported in Fig. 3). Initially, a short-lived Antarctic sea-ice area increase occurs approximately within the first two post-eruption years, which is not accompanied by a significant increase in sea-ice volume. This means that, in contrast to the Arctic sea-ice response, there is no post-eruption net build up of Antarctic sea-ice mass. As we will further discuss in Sect. 3.3, the areal expansion likely results in good part from a dynamic response of the Southern Ocean’s sea ice, which is advected over a larger area. This initial expansion phase is followed by a rebound retraction phase of similar amplitude and longer duration (Fig. 3b), which is characterized by a drastic reduction

Inter-hemispheric asymmetry in the sea-ice response to volcanic forcing

D. Zanchettin et al.

Title Page

Abstract

Introduction

Conclusions

References

Tables

Figures



Back

Close

Full Screen / Esc

Printer-friendly Version

Interactive Discussion



Inter-hemispheric asymmetry in the sea-ice response to volcanic forcing

D. Zanchettin et al.

Title Page

Abstract

Introduction

Conclusions

References

Tables

Figures

⏪

⏩

◀

▶

Back

Close

Full Screen / Esc

Printer-friendly Version

Interactive Discussion

in the total sea-ice volume (Fig. 3d). Note, reduction in sea-ice volume starts in year 1, when the positive anomaly in sea-ice area is near its peak, meaning that net losses in volume occurs already during the horizontally expanded phase of Antarctic sea ice. In other words, Antarctic sea ice covers a larger area while thinning. This second phase consistently ends about eight years after the eruption. Negative anomalies of both sea-ice area and volume are larger for SUPER1, whose ensemble-spread nonetheless overlaps with that of SUPER2 during the full duration of the rebound fluctuation.

Generally, ensemble-spreads are larger in the Antarctic sea-ice area estimates than in their Arctic counterparts. This is true also for the spread in sea-ice volume in its relative estimates, but not in its absolute values due to smaller Antarctic climatology (Fig. 3c and d). Overall, the post-eruption sea-ice evolution appears to be characterized by two distinct phases in the “supervolcano” ensembles: (i) an initial phase of tendential synchronic bi-polar expansion during integration years 1 and 2, and (ii) a subsequent, prolonged phase of inter-hemispheric asymmetry during integration years 4–6.

The anomalies determining the two detected phases of post-eruption sea-ice evolution feature a prominent seasonal character (Fig. 4). In the historical ensembles, the significant signals detected in the deseasonalized and smoothed series of total Arctic sea-ice area (Fig. 3a) originate from a significant increase during the boreal summer season (Fig. 4a). In the “supervolcano” ensembles the initial post-eruption increase in total Arctic sea-ice area occurs throughout the whole year but the magnitude of departures from the climatology is more than doubled in the boreal summer compared to the boreal winter. As we will show in Sect. 3.3, this behavior is most likely due to reduced melting, i.e. thermodynamics is very important for the initial response of Arctic sea ice to volcanic forcing. Predominance of reduced summer melting on winter growth is smeared out in the Arctic delayed response, and the annual cycle averaged over years 4–6 essentially corresponds to an upward-shifted unper-turbed annual cycle (Fig. 4c). By contrast, the signals in total Antarctic sea-ice area are largest in the sea-ice growth season (Fig. 4b), with initial post-eruption gains peaking at

~ 1.9–2.4 million km² in June–July and following losses peaking at ~ 1.8–2 million km² in August–October (Fig. 4d).

Figures 5 and 6 illustrate the regional distribution of sea-ice concentration anomalies for, respectively, the Arctic and the Antarctic region during the two detected phases of post-eruption sea-ice evolution for the SUPER1 ensemble. Mapped values refer to monthly anomalies at the end of the growing season (i.e. March for Arctic sea ice, September for Antarctic sea ice) and of the melting season (i.e. September for Arctic sea ice, March for Antarctic sea ice). Immediately after the eruption, the March Arctic sea-ice concentration increases especially in the gulf of Alaska/eastern Bering Sea and in the outer Labrador Sea/western North Atlantic, where the sea-ice edge significantly advances (Fig. 5a). Widespread reduced melting results in extensive increases in September Arctic sea-ice concentrations. These are particularly large in the Canadian Arctic Archipelago and in the Baffin Bay, where the sea-ice edge advances as far as reaching the Hudson and Davis Straits, along the East Greenland current, and in the Barents and Kara Seas, with the latter basin being fully sea-ice covered (Fig. 5c). The same regions are important for the total Arctic sea-ice area anomaly in the second phase of the post-eruption areal evolution of sea ice. Then, the strongest contribution to the winter anomaly of Arctic total sea-ice area comes from the North Atlantic/Nordic Seas sector, where March sea-ice concentrations increase by as much as 60 % (Fig. 5b). September Arctic sea-ice concentration anomalies are also still significant over extensive regions, but with overall smaller amplitudes (Fig. 5d).

In the Antarctic, total sea-ice area anomalies are of reduced amplitude and extension in austral summer during both phases (Fig. 4b and d). Immediately after the eruption, there is a circumpolar tendency towards positive March anomalies of sea-ice concentration, though these are strongest and most extensive off the West Antarctic coast, where they result in a local advance of the sea-ice edge (Fig. 6a). Later on, the same region faces a marked reduction of March sea-ice concentrations and a consequent retreat of the sea-ice edge (Fig. 6b), which is again part of a general circumpolar tendency. The regional details of September anomalies of Antarctic sea-ice concentration

ESDD

5, 121–168, 2014

Inter-hemispheric asymmetry in the sea-ice response to volcanic forcing

D. Zanchettin et al.

Title Page

Abstract

Introduction

Conclusions

References

Tables

Figures



Back

Close

Full Screen / Esc

Printer-friendly Version

Interactive Discussion



Inter-hemispheric asymmetry in the sea-ice response to volcanic forcing

D. Zanchettin et al.

Title Page

Abstract

Introduction

Conclusions

References

Tables

Figures



Back

Close

Full Screen / Esc

Printer-friendly Version

Interactive Discussion

during the two phases provide a more complex picture (Fig. 6c and d). In both phases, negative sea-ice concentration anomalies are diagnosed off the East Antarctic coasts and in the outer Weddell Sea. In the latter region, the response has the typical traits of an open-ocean polynya, i.e. an ice-free area within the ice cover, and is surrounded by positive anomalies leading to a locally advancing sea-ice edge during the initial post-eruption phase (Fig. 6c). Anomalies spatially extend more widely in the second phase, when a general retreat of the sea-ice edge is diagnosed (Fig. 6d). Whereas no significant large-scale changes are detected west of the Antarctic Peninsula in the initial phase (Fig. 6c), the same region faces later a reduction in sea-ice concentration which is locally as large as 60 % and results in a strong retreat of the sea-ice edge (Fig. 6d). Whereas both phases indicate reductions in September sea-ice concentrations in the outer Ross Sea, the initial post-eruption phase entails also an extensive increase along 60° S (Fig. 6c).

Differences between the shown SUPER1 patterns and their SUPER2 analogs (not shown) are generally minor. For historical eruptions, significant post-eruption sea-ice concentration anomalies are usually local, but generally point towards an agreement with the “supervolcano” ensembles concerning the tendencies in the key regions (not shown).

In summary, the sea-ice response to volcanic eruptions in MPI-ESM-COSMOS-Mill strongly depends on the amplitude of the induced global perturbation and, to a lesser extent, the location of the eruption (compare, e.g. the Arctic sea-ice response to the SUPER1/tropical and SUPER2/mid-latitude eruptions). All ensembles feature a temporary post-eruption increase in Arctic sea-ice, while no robust signature on Antarctic sea ice characterizes historical-size eruptions. The post-eruption sea-ice evolution in “supervolcano” simulations can be clearly separated into two phases: an initial one of bi-polar expansion and a delayed one marked by the contrast between persisting Arctic expansion and strong Antarctic contraction. The latter constitutes a counterintuitive simulated behavior, whose explanation seemingly lies in the anomalous seasonal behavior in a few key regions. This is explored further in the next section.

3.3 Mechanism of Arctic and Antarctic sea-ice response to a “supervolcano” eruption

In this section, we focus on the mechanism(s) behind the sea-ice response to the SUPER1 eruption during the initial bi-polar synchronic phase and the subsequent inter-hemispheric asymmetric phase. The SUPER1 ensemble is chosen among the two “supervolcano” eruptions since previous studies on the same ensemble (Timmreck et al., 2010, 2012) provide context to our inferences.

Significant decadal anomalies characterize the post-eruption evolutions of zonal-mean surface temperature and its associated hemispheric meridional gradients (Fig. 7a). The post-eruption anomalies depict: (i) strong initial cooling, mostly related to quick responses over the landmasses; (ii) bipolar asymmetry in the form of delayed and prolonged (compared to tropical regions) cooling in the Arctic contrasting the reduced cooling and subsequent warming in the Antarctic; (iii) inter-hemispheric asymmetry in the equator-to-pole temperature gradient, in the form of a temporarily strengthened gradient in the Northern Hemisphere contrasting a prolonged weakened gradient in the Southern Hemisphere; (iv) delayed (compared to both tropical and polar regions) cooling in the equatorial band, seemingly “phasing” ENSO to a La Niña state in year 3. The latter feature is associated to a temporary reduction of meridional gradients, which feature at this stage highly significant negative anomalies in the Southern Hemisphere.

Significant changes in the large-scale mid-tropospheric circulation are confined to the first 5–6 post-eruption years. Changes in the zonal-mean zonal winds describe a general weakening of the tropical and mid-latitude circulation of both hemispheres, though persisting longer in the Southern Hemisphere (Fig. 7b). This is concomitant with short-lived anomalous eastward polar circulations, which we interpret as part of the downward propagation of the volcanically-forced strengthened stratospheric polar vortices (not shown). Zonal-mean meridional winds at their climatological hemispheric maxima around 30° N and 50° S depict a significant reduction of the zonal-mean northward flow in years 1–2 in the Northern Hemisphere and a significant though rather

Inter-hemispheric asymmetry in the sea-ice response to volcanic forcing

D. Zanchettin et al.

Title Page

Abstract

Introduction

Conclusions

References

Tables

Figures



Back

Close

Full Screen / Esc

Printer-friendly Version

Interactive Discussion



Inter-hemispheric asymmetry in the sea-ice response to volcanic forcing

D. Zanchettin et al.

Title Page

Abstract

Introduction

Conclusions

References

Tables

Figures



Back

Close

Full Screen / Esc

Printer-friendly Version

Interactive Discussion

small increase of the zonal-mean southward flow in years 5–6 in the Southern Hemisphere (Fig. 7c). In the first two post-eruption years, the zonal and meridional wind response can be traced back to significant weakening of both the Hadley and Ferrell cells (not shown) consistent with a slow-down of the global hydrological cycle (compare Fig. 2b). During the second phase, zonal-mean vertical velocities depict a different behavior in the two hemispheres: during boreal summer the Northern Hemisphere features, as most prominent feature, a small though significant weakening of the upper and descending branches of the Hadley cell; during austral summer, the Southern Hemisphere features an expanded polar cell (not shown) consistent with the diagnosed changes in the meridional winds (Fig. 7c).

The anomalous atmospheric energy and oceanic heat transports into the polar regions (Fig. 8) provide constraints to our causal interpretation of the diagnosed regional changes. In the Northern Hemisphere, significant (i.e. outside the internal variability range) and prolonged reductions in the meridional heat transport into the Arctic region are diagnosed for both the atmosphere and the ocean: the reduction in atmospheric heat transport peaks at around lag 24 months and remains at significant levels over a 6 yr period; oceanic heat transport is reduced below the lower threshold of internal variability around lag 24 months and persists in an anomalously low state for almost one decade. The estimated dry static atmospheric energy transport remains generally within the internal variability range, with a less clear ensemble-mean evolution compared to the moist static energy transport (Fig. 8a). This indicates that the latent heat component – entailing reduced global ocean losses to the atmosphere (not shown) and reduced global precipitation (Fig. 2b) – dominates the response over the thermal component. At this latitude, the post-eruption anomalous oceanic heat transport is dominated by the gyre component (Fig. 8b), which agrees with the general behavior typically simulated by MPI-ESM-COSMOS-Mill (e.g. Zanchettin et al., 2012, 2013).

In the Southern Hemisphere, the atmospheric energy transport into the Antarctic region is significantly reduced between about 2 and 8 yr after the eruption (Fig. 8c), reflecting the evolution of anomalous equator-to-pole surface temperature gradient

**Inter-hemispheric
asymmetry in the
sea-ice response to
volcanic forcing**

D. Zanchettin et al.

Title Page

Abstract

Introduction

Conclusions

References

Tables

Figures

⏪

⏩

◀

▶

Back

Close

Full Screen / Esc

Printer-friendly Version

Interactive Discussion



(Fig. 7a). In absolute values, the associated peak post-eruption anomaly is about half of its Arctic counterpart (compare Fig. 8a and c). An initial, short-lived response is diagnosed in the estimated dry static atmospheric energy transport, compatible with the surface and tropospheric cooling simulated around these latitudes (compare Fig. 7a), which is evidently compensated by an increase in the atmospheric latent heat component. Oceanic heat transport into the Antarctic is characterized by strong interannual variability in its post-eruption anomalous evolution as well as by strong internal variability compared to its Arctic counterpart (compare ranges in Fig. 8b and d). As a consequence, despite peak anomalies about twice those diagnosed in the Arctic, the post-eruption ocean heat transport into the Antarctic remains mostly within the internal variability range. The most significant feature is a temporary reduction in the total poleward transport around lag of 48 months (Fig. 8d). As for the Northern Hemisphere, at these latitudes oceanic transport is dominated by the gyre component.

In summary, both polar regions feature a post-eruption decrease in the energy import. However, the decrease is overall more significant for the Arctic due to an overall more constrained oceanic internal variability range and to constructively superposing and comparable contributions from the atmosphere and the ocean, the former being pivotal in the initial response phase and the latter dominating the response thereafter. For the Antarctic, both oceanic and moist atmospheric energy transports remain initially unaffected, pointing towards dynamical circulation changes as cause for the initial Antarctic sea-ice response. Furthermore, the relevance of the ocean for the post-eruption Antarctic energy budget and its attribution to the imposed forcing is hampered by its strong internal variability. It is therefore important to relate anomalous ocean meridional heat transports to dynamical changes in the oceanic circulation.

In the Northern Hemisphere, the general response of the oceanic circulation to the SUPER1 eruption is in line with the behavior typically simulated by MPI-ESM-COSMOS-Mill after historical-size eruptions (see, e.g. Zanchettin et al., 2012, 2013). We therefore only show changes more closely related to sea ice. The post-eruption reduction in gyre-driven northward heat transport is clearly associated with a weakening

be regarded as mainly a consequence of local coupled ocean-atmosphere dynamics internal to the Antarctic region. The consistency with corresponding anomalous patterns in the SUPER2 ensemble (not shown) adds support to this interpretation.

Enhanced deep convection still takes place in the Weddell Sea region during the second response phase (Fig. 10d), though its magnitude and extent are reduced compared to the initial anomaly. Again, the causal chain for this behavior cannot be fully clarified based on our experiments alone allowing for tentative hypotheses only. We accordingly interpret the strengthened oceanic convection as a likely consequence of locally strengthened surface exchange processes (Fig. 12c) favored by the meanwhile decreased winter sea-ice area (Fig. 6d). We thus regard the negative sea-ice anomaly as the closure element of the feedback mechanism characterizing the post-eruption ocean-atmosphere evolution in the Weddell Sea region (i.e. the regional anomaly persists until the anomalous large-scale atmospheric circulation sustains a local sea-ice reduction).

4 Summarizing discussion

In this study we used ensemble climate simulations performed with the COSMOS-Mill version of the Max Planck Institute-Earth System Model (MPI-ESM) to investigate the decadal response of Arctic and Antarctic sea ice to volcanic perturbations. We considered volcanic eruptions of different magnitude, ranging from historical-size to “supervolcano”-size, the latter with different characteristics, including tropical and extra-tropical locations. In all ensembles a sustained, largely thermally-driven expansion is robustly simulated for total area and volume of Arctic sea ice. Amplitude and duration of the anomalies essentially depend on the magnitude of the imposed forcing. In contrast, the simulated response of Antarctic sea ice is elusive for the historical-size eruptions, while “supervolcano” eruptions induce an initial short-lived, mostly dynamically-driven Antarctic sea-ice expansion which is followed by a prolonged retraction phase.

Inter-hemispheric asymmetry in the sea-ice response to volcanic forcing

D. Zanchettin et al.

Title Page

Abstract

Introduction

Conclusions

References

Tables

Figures

⏪

⏩

◀

▶

Back

Close

Full Screen / Esc

Printer-friendly Version

Interactive Discussion



For both historical and “supervolcano” eruption-types we diagnose, therefore, an inter-hemispheric asymmetry in the simulated post-eruption decadal evolution of sea ice.

In the case of a “supervolcano” eruption, the asymmetry primarily derives from the different sensitivity of Arctic and Antarctic regional climates to the induced global energy imbalance and from the associated large-scale atmospheric and oceanic dynamical reactions. Thermodynamics is the key for the Arctic sea-ice expansion, which is triggered by the initially reduced atmospheric heat import and is then sustained on a decadal time scale by the meanwhile reduced oceanic heat import. Noteworthy, decadal responses of North Atlantic/Arctic large-scale oceanic circulation are qualitatively similar for historical and “supervolcano” eruptions, both including a delayed strengthening of the AMOC and a north-westward compression of the subpolar gyre (compare Fig. 9b with Zanchettin et al., 2012). For the “supervolcano” eruptions, however, the post-eruption drop in the heat content of the global upper ocean is too large to allow for circulation-driven positive anomalies of ocean heat transport into the Arctic, as diagnosed for historical eruptions (see Zanchettin et al., 2012, 2013).

In contrast to Arctic sea ice, Antarctic sea ice reacts on the short-term mostly to dynamical atmospheric changes initiated by the volcanically-induced strengthening of the Southern Hemisphere’s stratospheric polar vortex. Antarctic sea ice is thereafter implicated in local surface energy exchange processes dominating the response diagnosed at the hemispheric scale. The post-eruption anomalies of lateral oceanic heat flux are larger in the Antarctic than in the Arctic, but they only temporarily exceed the internal variability range (Fig. 8d). We regard the temporarily, significantly decreased poleward oceanic heat transport around year 4 as a marginal contributor to the Antarctic sea-ice anomaly (negative at this stage). Post-eruption negative anomalies of atmospheric energy fluxes are likely a consequence of rather than a cause of the chain of local feedbacks within the Antarctic region. The substantially different exposure of the Arctic and Antarctic regional climates to volcanically-forced energy imbalances explains why the inter-hemispheric asymmetry becomes apparent with increasing magnitude of the eruption.

Inter-hemispheric asymmetry in the sea-ice response to volcanic forcing

D. Zanchettin et al.

Title Page

Abstract

Introduction

Conclusions

References

Tables

Figures



Back

Close

Full Screen / Esc

Printer-friendly Version

Interactive Discussion



**Inter-hemispheric
asymmetry in the
sea-ice response to
volcanic forcing**

D. Zanchettin et al.

Title Page

Abstract

Introduction

Conclusions

References

Tables

Figures



Back

Close

Full Screen / Esc

Printer-friendly Version

Interactive Discussion



In both the Arctic and the Antarctic, regions of strongest simulated sea-ice response correspond to key regions for sea-ice and ice-cap variability found in reconstructions and observations. For instance, extensive increases in September Arctic sea-ice concentrations are simulated in the Canadian Arctic Archipelago and in the Baffin Bay (Fig. 5c). This is in agreement with records of ice-cap growth from Arctic Canada covering the last millennium indicating a strong link to large volcanic eruptions (Anderson et al., 2008; Miller et al., 2012). In our simulations, internal variability of Antarctic sea ice is stronger for total area and weaker for total volume compared to Arctic sea ice (Fig. 3, note that total Antarctic sea-ice volume is almost half its Arctic counterpart). As shown by the forced responses, hemispheric metrics for the Antarctic often mask strong spatially-heterogeneous variability (Fig. 6c), as also indicated by observations (e.g. Simpkins et al., 2012, 2013). The interplay between large-scale dynamics and local processes highlights several relevant mechanisms and features, which need to be reliably represented in models to build confidence in the simulated representation of post-eruption sea-ice evolutions, particularly for the Antarctic. These include, among others, the global hydrological cycle, the downward propagation of polar vortex signals, ENSO, the global oceanic conveyor of heat, and the atmospheric forcing of the Antarctic circumpolar current (ACC).

The downward propagation of volcanically-forced stratospheric signals, especially the post-eruption strengthening of the stratospheric polar vortex, is important for the initial dynamical atmospheric response to explosive volcanic eruptions (e.g. Stenchikov et al., 2006; Fischer et al., 2007; Zanchettin et al., 2012). The stratospheric polar vortex significantly strengthens after the eruption in both hemispheres in HIST2, SUPER1 and SUPER2, with duration tracing that of the imposed radiative anomaly, but it does not in HIST1 (not shown). Signals in the polar mid-troposphere are robust only for “super-volcano” eruptions (compare Fig. 7b). Larger ensembles could fully clarify whether the lack of robust dynamical atmospheric responses for historical eruptions reflects a low signal-to-noise ratio rather than a truly lacking dynamical response. The latter hypothesis, however, is supported by the deficient representation of stratospheric dynamics

and stratospheric-tropospheric coupling in latest-generation “low-top” coupled general circulation models (CGCMs) (Charlton-Perez et al., 2013; Omrani et al., 2014), a characteristic which is shared by the version of MPI-ESM used here.

Similar concerns arise about the simulated southern tropospheric mid-latitude jet, e.g. its too equatorward climatological position (e.g. Swart and Fyfe, 2012). Furthermore, simulated Antarctic sea-ice variability and sensitivity to external disturbances may as well suffer from an imperfect description of tropospheric internal dynamics, e.g. those related to variability of the Southern Annular Mode (Simpson et al., 2013) and of the associated surface wind variability (Zhang, 2014). In particular, the strength and latitudinal position of the circumpolar winds affect the Antarctic sea ice via the Ekman transport (Maksym et al., 2012; Landrum et al., 2012; Weijer et al., 2012). In our simulations the total Antarctic sea-ice volume does not support the early post-eruption horizontal expansion phase (Fig. 3b and d) leading to sea-ice thinning. This contrasts other model-based indications that wind intensification tends to increase Antarctic sea-ice volume through increased ridged ice production (Zhang, 2014). The post-eruption initial resilience of total Antarctic sea-ice volume may therefore reflect a truly distinct dynamical behavior related to extremely strong volcanic forcing, but it may also reflect poor representation of near-surface atmospheric circulation. This is important for the case discussed here, given also the marked seasonal character of Antarctic sea-ice response to the volcanic perturbation during the delayed contraction phase (Fig. 4d).

The timing of the strongest post-eruption surface cooling at equatorial latitudes, delayed with respect to that at mid-latitudes, strongly contributes to the post-eruption strengthening of meridional gradients (Fig. 7). This equatorial cooling has a strong imprint in the Pacific in the form of an apparent phasing of ENSO on a delayed La Niña state. This robust response of ENSO to the volcanic perturbation occurs after the maximum global surface cooling (compare with Fig. 2a), when the Toba/SUPER1 ensemble indicates a non-significant, though tendentially warm, ENSO response (Timmreck et al., 2010). ENSO in this version of MPI-ESM was consistently found to be only weakly sensitive to volcanic forcing for a selection of historical-size eruptions

Inter-hemispheric asymmetry in the sea-ice response to volcanic forcing

D. Zanchettin et al.

Title Page

Abstract

Introduction

Conclusions

References

Tables

Figures



Back

Close

Full Screen / Esc

Printer-friendly Version

Interactive Discussion

Inter-hemispheric asymmetry in the sea-ice response to volcanic forcing

D. Zanchettin et al.

Title Page

Abstract

Introduction

Conclusions

References

Tables

Figures

◀

▶

◀

▶

Back

Close

Full Screen / Esc

Printer-friendly Version

Interactive Discussion

- Brohan, P., Kennedy, J. J., Harris, I., Tett, S. F. B., and Jones, P. D.: Uncertainty estimates in regional and global observed temperature changes: a new dataset from 1850, *J. Geophys. Res.*, 111, D12106, doi:10.1029/2005JD006548, 2006.
- Charlton-Perez, A. J., Baldwin, M. P., Birner, T., Black, R. X., Butler, A. H., Calvo, N., Davis, N. A., Gerber, E. P., Gillett, N., Hardiman, S., Kim, J., Krüger, K., Lee, Y.-Y., Manzini, E., McDaniel, B. A., Polvani, L., Reichler, T., Shaw, T. A., Sigmund, M., Son, S.-W., Toohey, M., Wilcox, L., Yoden, S., Christiansen, B., Lott, F., Shindell, D., Yukimoto, S., and Watanabe, S.: On the lack of stratospheric dynamical variability in low-top versions of the CMIP5 models, *J. Geophys. Res.*, 118, 2494–2505, doi:10.1002/jgrd.50125, 2013.
- Chylek, P., Folland, C. K., Lesins, G., and Dubey, M. K.: Twentieth century bipolar seesaw of the Arctic and Antarctic surface air temperatures, *Geophys. Res. Lett.*, 37, L08703, doi:10.1029/2010GL042793, 2010.
- Crowley, T. J. and Unterman, M. B.: Technical details concerning development of a 1200 yr proxy index for global volcanism, *Earth Syst. Sci. Data*, 5, 187–197, doi:10.5194/essd-5-187-2013, 2013.
- Crowley, T. J., Zielinski, G., Vinther, B., Udisti, R., Kreutz, K., Cole-Dai, J., and Castellano, E.: Volcanism and the little ice age, *PAGES News*, 16, 22–23, 2008.
- Duncan, R. P., Fenwick, P., Palmer, J. G., McGlone, M. S., and Turney, C. S. M.: Non-uniform interhemispheric temperature trends over the past 550 years, *Clim. Dynam.*, 35, 1429–1438, doi:10.1007/s00382-010-0794-2, 2010.
- Fischer, E., Luterbacher, J., Zorita, E., Tett, S. F. B., Casty, C., and Wanner, H.: European climate response to tropical volcanic eruptions over the last half millennium, *Geophys. Res. Lett.*, 34, L05707, doi:10.1029/2006GL027992, 2007.
- Graf, H. F. and Zanchettin, D.: Central Pacific El Niño, the “subtropical bridge” and Eurasian Climate, *J. Geophys. Res.*, 117, D01102, doi:10.1029/2011JD016493, 2012.
- Griffies, S. M., Biastoch, A., Böning, C., Bryan, F., Danabasoglu, G., Chassignet, E. P., England, M. P., Gerdes, R., Haak, H., Hallberg, R. W., Hazeleger, W., Jungclaus, J., Large, W. G., Madec, G., Pirani, A., Samuels, B. L., Scheinert, M., Gupta, A. S., Severijns, C. A., Simmons, H. L., Treguier, A. M., Winton, M., Yeager, S., and Yin, J.: Coordinated Ocean-ice Reference Experiments (COREs), *Ocean Model.*, 26, 1–46, doi:10.1016/j.ocemod.2008.08.007, 2009.
- Gulyardi, E., Wittenberg, A., Fedorov, A., Collins, M., Wang, C. Z., Capotondi, A., van Oldenborgh, G. J., and Stockdale, T.: Understanding El Niño in ocean-atmosphere General Circulation Models: progress and challenges, *B. Am. Meteorol. Soc.*, 90, 325–340, 2009.

Inter-hemispheric asymmetry in the sea-ice response to volcanic forcing

D. Zanchettin et al.

Title Page

Abstract

Introduction

Conclusions

References

Tables

Figures

◀

▶

◀

▶

Back

Close

Full Screen / Esc

Printer-friendly Version

Interactive Discussion

Heuzé, C., Heywood, K. J., Stevens, D. P., and Ridley, J. K.: Southern Ocean bottom water characteristics in CMIP5 models, *Geophys. Res. Lett.*, 40, 1409–1414, doi:10.1002/grl.50287, 2013.

Holden, P. B., Edwards, N. R., Wolff, E. W., Lang, N. J., Singarayer, J. S., Valdes, P. J., and Stocker, T. F.: Interhemispheric coupling, the West Antarctic Ice Sheet and warm Antarctic interglacials, *Clim. Past*, 6, 431–443, doi:10.5194/cp-6-431-2010, 2010.

Jones, G. S., Gregory, J. M., Stott, P. A., Tett, S. F. B., and Thorpe, R. B.: An AOGCM simulation of the climate response to a volcanic super-eruption, *Clim. Dynam.*, 25, 725–738, 2005.

Jungclaus, J. H., Keenlyside, N., Botzet, M., Haak, H., Luo, J. J., Latif, M., Marotzke, J., Mikolajewicz, U., and Roeckner, F.: Ocean circulation and tropical variability in the coupled model ECHAM5/MPI-OM, *J. Climate*, 19, 3952–3972, 2006.

Jungclaus, J. H., Lorenz, S. J., Timmreck, C., Reick, C. H., Brovkin, V., Six, K., Segschneider, J., Giorgetta, M. A., Crowley, T. J., Pongratz, J., Krivova, N. A., Vieira, L. E., Solanki, S. K., Klocke, D., Botzet, M., Esch, M., Gayler, V., Haak, H., Raddatz, T. J., Roeckner, E., Schnur, R., Widmann, H., Claussen, M., Stevens, B., and Marotzke, J.: Climate and carbon-cycle variability over the last millennium, *Clim. Past*, 6, 723–737, doi:10.5194/cp-6-723-2010, 2010.

Jungclaus, J. H., Fischer, N., Haak, H., Lohmann, K., Marotzke, J., Matei, D., Mikolajewicz, U., Notz, D., and von Storch, J.: Characteristics of the ocean simulations in MPIOM, the ocean component of the MPI-Earth system model, *J. Adv. Model. Earth Syst.*, 5, 422–446, doi:10.1002/jame.20023, 2013.

Karpechko, A. Y., Gillett, N. P., Dall’Amico, M., and Gray, L. J.: Southern Hemisphere atmospheric circulation response to the El Chichón and Pinatubo eruptions in coupled climate models, *Q. J. Roy. Meteorol. Soc.*, 136, 1813–1822, doi:10.1002/qj.683, 2010.

Keith, D. W.: Meridional energy transport: uncertainty in zonal means, *Tellus A*, 47, 30–44, 1995.

Kinnard, G., Zdanowicz, C. M., Fisher, D. A., Isakkson, E., de Vernal, A., and Thompson, L. G.: Reconstructed changes in Arctic sea ice over the past 1450 years, *Nature*, 479, 509–513, doi:10.1038/nature10581, 2011.

Kirkman, C. and Bitz, C. M.: The effect of the sea ice freshwater flux on southern ocean temperatures in CCSM3: deep ocean warming and delayed surface warming, *J. Climate*, 24, 2224–2237 doi:10.1175/2010JCLI3625.1, 2011.

Inter-hemispheric asymmetry in the sea-ice response to volcanic forcing

D. Zanchettin et al.

Title Page

Abstract

Introduction

Conclusions

References

Tables

Figures

⏪

⏩

◀

▶

Back

Close

Full Screen / Esc

Printer-friendly Version

Interactive Discussion

- Landrum, L., Holland, M. M., Schneider, D. P., and Hunke, E.: Antarctic sea ice climatology, variability, and late twentieth-century change in CCSM4, *J. Climate*, 25, 4817–4838, doi:10.1175/JCLI-D-11-00289.1, 2012.
- Li, J., Xie, S.-P., Cook, E. R., Morales, M. S., Christie, D. A., Johnson, N. C., Chen, F., D'Arrigo, R., Fowler, A. M., Gou, X., and Fang, K.: El Niño modulations over the past seven centuries, *Nat. Clim. Change*, 3, 822–826, doi:10.1038/NCLIMATE1936, 2013.
- Maksym, T., Stammerjohn, S. E., Ackley, S., and Massom, R.: Antarctic sea ice – a polar opposite?, *Oceanography*, 25, 140–151, doi:10.5670/oceanog.2012.88, 2012.
- Marshall, G. J.: Trends in the Southern Annular Mode from observations and reanalyses, *J. Climate*, 16, 4134–4143, doi:10.1175/1520-0442(2003)016<4134:TITSAM>2.0.CO;2, 2003.
- Marsland, S. J., Haak, H., Jungclaus, J. H., Latif, M., and Röske, F.: The Max Planck Institute global ocean/sea ice model with orthogonal curvilinear coordinates, *Ocean Model.*, 5, 91–127, 2003.
- Martin, T., Park, W., and Latif, M.: Multi-centennial variability controlled by Southern Ocean convection in the Kiel Climate Model, *Clim. Dynam.*, 40, 2005–2022, doi:10.1007/s00382-012-1586-7, 2013.
- Massonnet, F., Mathiot, P., Fichefet, T., Goosse, H., Beatty, C. K., Vancoppenolle, M., and Lavergne, T.: Model reconstruction of the Antarctic sea ice thickness and volume changes over 1980–2008 using data assimilation, *Ocean Model.*, 64, 67–75, doi:10.1016/j.ocemod.2013.01.003, 2013.
- Meier, W. N., Gallaher, D., and Campbell, G. G.: New estimates of Arctic and Antarctic sea ice extent during September 1964 from recovered Nimbus I satellite imagery, *The Cryosphere*, 7, 699–705, doi:10.5194/tc-7-699-2013, 2013.
- Miller, G. H., Geirsdóttir, Á., Zhong, Y., Larsen, D. J., Otto-Bliesner, B. L., Holland, M. M., Bailey, D. A., Refsnider, K. A., Lehman, S. J., Southon, J. R., Anderson, C., Björnsson, H., and Thordarson, T.: Abrupt onset of the Little Ice Age triggered by volcanism and sustained by sea-ice/ocean feedbacks, *Geophys. Res. Lett.*, 39, L02708, doi:10.1029/2011GL050168, 2012.
- Niemeier, U., Timmreck, C., Graf, H.-F., Kinne, S., Rast, S., and Self, S.: Initial fate of fine ash and sulfur from large volcanic eruptions, *Atmos. Chem. Phys.*, 9, 9043–9057, doi:10.5194/acp-9-9043-2009, 2009.
- Notz, D. and Marotzke, J.: Observations reveal external driver for Arctic sea-ice retreat, *Geophys. Res. Lett.*, 39, L08502, doi:10.1029/2012GL051094, 2012.

Inter-hemispheric asymmetry in the sea-ice response to volcanic forcing

D. Zanchettin et al.

Title Page

Abstract

Introduction

Conclusions

References

Tables

Figures

◀

▶

◀

▶

Back

Close

Full Screen / Esc

Printer-friendly Version

Interactive Discussion

- Omrani, N.-E., Keenlyside, N., Bader, J., and Manzini, E.: Stratosphere key for wintertime atmospheric response to warm Atlantic decadal conditions, *Clim. Dynam.*, 42, 649–663, doi:10.1007/s00382-013-1860-3, 2014.
- Park, W. and Latif, M.: Multidecadal and multicentennial variability of the meridional overturning circulation, *Geophys. Res. Lett.*, 35, L22703, doi:10.1029/2008GL035779, 2008.
- Parkinson, C. L.: Southern Ocean sea ice and its wider linkages: insights revealed from models and observations, *Antarct. Sci.*, 16, 387–400, doi:10.1017/S0954102004002214, 2004.
- Polvani, L. M. and Smith, K. L.: Can natural variability explain observed Antarctic sea ice trends? New modeling evidence from CMIP5, *Geophys. Res. Lett.*, 40, 3195–3199, doi:10.1002/grl.50578, 2013.
- Raddatz, T. J., Reick, C. H., Knorr, W., Kattge, J., Roeckner, E., Schnur, R., Schnitzler, K.-G., Wetzol, P., and Jungclaus, J.: Will the tropical land biosphere dominate the climate-carbon cycle feedback during the twenty-first century?, *Clim. Dynam.*, 29, 565–574, 2007.
- Robock, A., Adams, T., Moore, M., Oman, L., and Stenchikov, G.: Southern Hemisphere atmospheric circulation effects of the 1991 Mount Pinatubo eruption, *Geophys. Res. Lett.*, 34, L23710, doi:10.1029/2007GL031403, 2007.
- Roeckner, E., Brokopf, R., Esch, M., Giorgetta, M., Hagemann, S., Kornblueh, L., Manzini, E., Schlese, U., and Schulzweida, U.: Sensitivity of simulated climate to horizontal and vertical resolution in the ECHAM5 atmosphere model, *J. Climate*, 19, 3771–3791, doi:10.1175/JCLI3824.1, 2006.
- Russell, J. L., Stouffer, R. J., and Dixon, K. W.: Intercomparison of the Southern Ocean Circulations in IPCC Coupled Model Control Simulations, *J. Climate*, 19, 4560–4575, 2006.
- Sallée, J.-B., Shuckburgh, E., Bruneau, N., Meijers, A. J. S., Bracegirdle, T. J., and Wang, Z.: Assessment of Southern Ocean mixed layer depths in CMIP5 models: historical bias and forcing response, *J. Geophys. Res.-Oceans*, 118, 1845–1862, doi:10.1002/jgrc.20157, 2013.
- Schaefer, J. M., Denton, G. H., Kaplan, M., Putnam, A., Finkel, R. C., Barrell, D. J. A., Andersen, B. G., Schwartz, R., Mackintosh, A., Chinn, T., and Schlüchter, C.: High-frequency Holocene glacier fluctuations in New Zealand differ from the northern signature, *Science*, 324, 622–625, 2009.
- Schleussner, C. F. and Feulner, G.: A volcanically triggered regime shift in the subpolar North Atlantic Ocean as a possible origin of the Little Ice Age, *Clim. Past*, 9, 1321–1330, doi:10.5194/cp-9-1321-2013, 2013.

Inter-hemispheric asymmetry in the sea-ice response to volcanic forcing

D. Zanchettin et al.

Title Page

Abstract

Introduction

Conclusions

References

Tables

Figures

◀

▶

◀

▶

Back

Close

Full Screen / Esc

Printer-friendly Version

Interactive Discussion

- Segschneider, J., Beitsch, A., Timmreck, C., Brovkin, V., Ilyina, T., Jungclaus, J., Lorenz, S. J., Six, K. D., and Zanchettin, D.: Impact of an extremely large magnitude volcanic eruption on the global climate and carbon cycle estimated from ensemble Earth System Model simulations, *Biogeosciences*, 10, 669–687, doi:10.5194/bg-10-669-2013, 2013.
- 5 Shakun, J. D., Clark, P. U., He, F., Marcott, S. A., Mix, A. C., Liu, Z., Otto-Bliesner, B., Schmittner, A., and Bard, E.: Global warming preceded by increasing carbon dioxide concentrations during the last deglaciation, *Nature*, 484, 49–54, doi:10.1038/nature10915, 2012.
- Shin, S.-I., Liu, Z., Otto-Bliesner, B. L., Kutzbach, J. E., and Vavrus, S. J.: Southern Ocean sea-ice control of the glacial North Atlantic thermohaline circulation, *Geophys. Res. Lett.*, 30, 1096, doi:10.1029/2002GL015513, 2003.
- 10 Simpkins, G. R., Ciasto, L. M., Thompson, D. W. J., and England, M. H.: Seasonal relationships between large-scale climate variability and Antarctic sea ice concentration, *J. Climate*, 25, 5451–5469, doi:10.1175/JCLI-D-11-00367.1, 2012.
- Simpkins, G. R., Ciasto, L. M., and England, M. H.: Observed variations in multidecadal Antarctic sea ice trends during 1979–2012, *Geophys. Res. Lett.*, 40, 1–6, doi:10.1002/grl.50715, 2013.
- 15 Simpson, I. R., Hitchcock, P., Shepherd, T. G., and Scinocca, J. F.: Southern Annular Mode Dynamics in Observations and Models, Part I: The Influence of Climatological Zonal Wind Bases in a Comprehensive GCM, *J. Climate*, 26, 3953–3967, doi:10.1175/JCLI-D-12-00348.1, 2013.
- 20 Stammerjohn, S., Massom, R., Rind, D., and Martinson, D.: Regions of rapid sea ice change: an inter-hemispheric seasonal comparison, *Geophys. Res. Lett.*, 39, L06501, doi:10.1029/2012GL050874, 2012.
- Stenchikov, G., Hamilton, K., Stouffer, R. J., Robock, A., Ramaswamy, V., Santer, B., and Graf, H.-F.: Arctic Oscillation response to volcanic eruptions in the IPCC AR4 climate models, *J. Geophys. Res.*, 111, D07107, doi:10.1029/2005JD006286, 2006.
- 25 Stenchikov, G., Delworth, T. L., Ramaswamy, V., Stouffer, R. J., Wittenberg, A., and Zeng, F.: Volcanic signals in oceans, *J. Geophys. Res.*, 114, D16104, doi:10.1029/2008JD011673, 2009.
- 30 Stier, P., Feichter, J., Kinne, S., Kloster, S., Vignati, E., Wilson, J., Ganzeveld, L., Tegen, I., Werner, M., Balkanski, Y., Schulz, M., Boucher, O., Minikin, A., and Petzold, A.: The aerosol-climate model ECHAM5-HAM, *Atmos. Chem. Phys.*, 5, 1125–1156, doi:10.5194/acp-5-1125-2005, 2005.

Inter-hemispheric asymmetry in the sea-ice response to volcanic forcing

D. Zanchettin et al.

Title Page

Abstract

Introduction

Conclusions

References

Tables

Figures

◀

▶

◀

▶

Back

Close

Full Screen / Esc

Printer-friendly Version

Interactive Discussion

- Stössel, A., Zhang, Z., and Vihma, T.: The effect of alternative real-time wind forcing on Southern Ocean sea-ice simulations, *J. Geophys. Res.*, 116, C11021, doi:10.1029/2011JC007328, 2011.
- Stouffer, R. J., Broccoli, A. J., Delworth, T. L., Dixon, K. W., Gudgel, R., Held, I., Hemler, R., Knutson, T., Lee, H.-C., Schwarzkopf, M. D., Soden, B., Spelman, M. J., Winton, M., and Zeng, F.: GFDL's CM2 global coupled climate models, Pt. IV: Idealized climate response, *J. Climate*, 19, 723–740, doi:10.1175/JCLI3632.1, 2006.
- Stroeve, J. C., Kattsov, V., Barrett, A. P., Serreze, M. C., Pavlova, T., Holland, M. M., and Meier, W. N.: Trends in Arctic sea ice extent from CMIP5, CMIP3 and observations, *Geophys. Res. Lett.*, 39, L16502, doi:10.1029/2012GL052676, 2012.
- Swart, N. C. and Fyfe, J. C.: Observed and simulated changes in Southern Hemisphere surface westerlies, *Geophys. Res. Lett.*, 39, L16711, doi:10.1029/2012GL052810, 2012.
- Thompson, D. W. J., Wallace, J. M., Jones, P. D., and Kennedy, J. J.: Identifying signatures of natural climate variability in time series of global-mean surface temperature: methodology and insights, *J. Climate*, 22, 6120–6141, 2009.
- Timmreck, C.: Modeling the climatic effects of large volcanic eruptions, *WIREs Clim. Change*, 3, 545–564, doi:10.1002/wcc.192, 2012.
- Timmreck, C., Lorenz, S. J., Crowley, T. J., Kinne, S., Raddatz, T. J., Thomas, M. A., and Jungclaus, J. H.: Limited temperature response to the very large AD 1258 volcanic eruption, *Geophys. Res. Lett.*, 36, L21708, doi:10.1029/2009GL040083, 2009.
- Timmreck, C., Graf, H.-F., Lorenz, S. J., Niemeier, U., Zanchettin, D., Matei, D., Jungclaus, J. H., and Crowley, T. J.: Aerosol size confines climate response to volcanic super-eruptions, *Geophys. Res. Lett.*, 37, L24705, doi:10.1029/2010GL045464, 2010.
- Timmreck, C., Graf, H.-F., Zanchettin, D., Hagemann, S., Kleinen, T., and Krüger, K.: Climate response to the Toba eruption: regional changes, *Quatern. Int.*, 258, 30–44, 2012.
- Turner, J., Bracegirdle, T. J., Phillips, T., Marshall, G. J., and Hosking, J. S.: An Initial Assessment of Antarctic Sea Ice Extent in the CMIP5 Models, *J. Climate*, 26, 1473–1484, doi:10.1175/JCLI-D-12-00068.1, 2013.
- Wang, M. and Overland, J. E. E.: A sea ice free summer Arctic within 30 years – an update from CMIP5 models, *Geophys. Res. Lett.*, 39, L18501, doi:10.1029/2012GL052868, 2012.
- Weber, M. E., Clark, P. U., Ricken, W., Mitrovica, J. X., Hostetler, S. W., and Kuhn, G.: Interhemispheric Ice-Sheet Synchronicity During the Last Glacial Maximum, *Science*, 334, 1265–1269, doi:10.1126/science.1209299, 2011.

Inter-hemispheric asymmetry in the sea-ice response to volcanic forcing

D. Zanchettin et al.

Title Page

Abstract

Introduction

Conclusions

References

Tables

Figures



Back

Close

Full Screen / Esc

Printer-friendly Version

Interactive Discussion



Weijer, W., Sloyan, B. M., Maltrud, M. E., Jeffery, N., Hecht, M. W., Hartin, C. A., van Sebille, E., Wainer, I., and Landrum, L.: The Southern Ocean and its climate in CCSM4, *J. Climate*, 25, 2652–2675, doi:10.1175/JCLI-D-11-00302.1, 2012.

Wetzel, P., Winguth, A., and Maier-Reimer, E.: Sea-to-air CO₂ fluxes from 1948 to 2003, *Global Biogeochem. Cy.*, 19, GB2005, doi:10.1029/2004GB002339, 2005.

Zanchettin, D., Timmreck, C., Graf, H.-F., Rubino, A., Lorenz, S., Lohmann, K., Krueger, K., and Jungclaus, J. H.: Bi-decadal variability excited in the coupled ocean–atmosphere system by strong tropical volcanic eruptions, *Clim. Dynam.*, 39, 1–2, 419–444, doi:10.1007/s00382-011-1167-1, 2012.

Zanchettin, D., Bothe, O., Graf, H. F., Lorenz, S. J., Luterbacher, J., Timmreck, C., and Jungclaus, J. H.: Background conditions influence the decadal climate response to strong volcanic eruptions. *J. Geophys. Res.-Atmos.*, 118, 4090–4106, doi:10.1002/jgrd.50229, 2013.

Zhang, J.: Increasing Antarctic sea ice under warming atmospheric and oceanic conditions, *J. Climate*, 20, 2515–2529, doi:10.1175/JCLI4136.1, 2007.

Zhang, J.: Modeling the Impact of Wind Intensification on Antarctic Sea Ice Volume, *J. Climate*, 27, 202–214, doi:10.1175/JCLI-D-12-00139.1, 2014.

Zhong, Y., Miller, G. H., Otto-Bliesner, B. L., Holland, M. M., Bailey, D. A., Schneider, D. P., and Geirsdottir, A.: Centennial-scale climate change from decadal-paced explosive volcanism: a coupled sea ice-ocean mechanism, *Clim. Dynam.*, 37, 2373–2387, doi:10.1007/s00382-010-0967-z, 2011.

Inter-hemispheric asymmetry in the sea-ice response to volcanic forcing

D. Zanchettin et al.

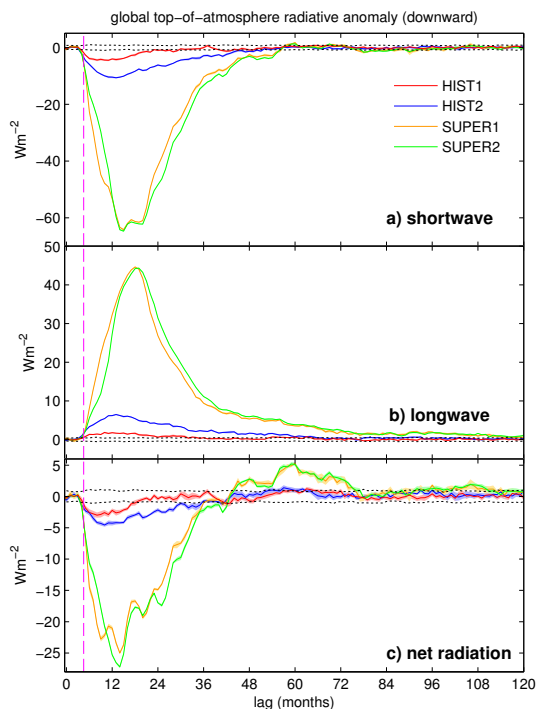


Fig. 1. Simulated imposed forcing in the two historical and the two “supervolcano” ensembles as diagnosed through anomalies in the global-average top-of-atmosphere solar (shortwave, **a**), thermal (longwave, **b**) and net (**c**) radiation. Lines (shading): mean (standard error of the mean). Black dotted lines indicate the internal variability range ($n = 10$, see methods). The magenta vertical hatched line indicates the approximate start of the eruptions. Lag(0) corresponds to January of the eruption year. Positive anomalies correspond to increased downward flux. No smoothing was applied to the series.

Inter-hemispheric asymmetry in the sea-ice response to volcanic forcing

D. Zanchettin et al.

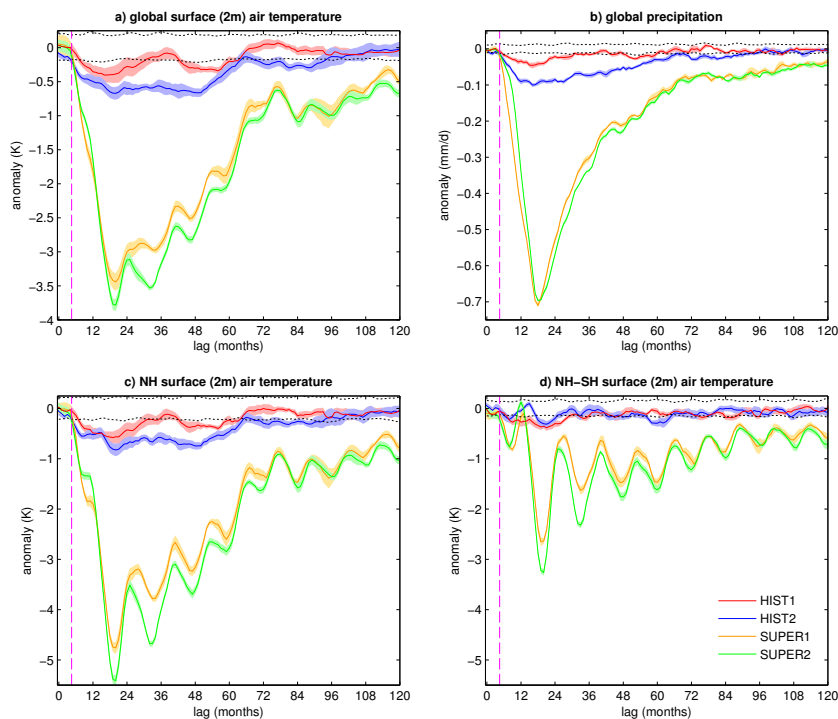


Fig. 2. Simulated post-eruption anomalies of global-average surface (2 m) air temperature (SAT) **(a)** and total precipitation **(b)**, and Northern-hemispheric average SAT **(c)** and difference between Northern and Southern-hemispheric average SAT **(d)** for the two historical and the two “supervolcano” ensembles. Lines (shading): mean (standard error of the mean). Black dashed lines indicate the internal variability range ($n = 10$, see methods). The magenta vertical hatched line indicates the approximate start of the eruptions. Lag(0) corresponds to January of the eruption year. Note that the y axis in **(c)** and **(d)** has the same scale, highlighting the relative magnitude of inter-hemispheric differences in the temperature response.

Inter-hemispheric asymmetry in the sea-ice response to volcanic forcing

D. Zanchettin et al.

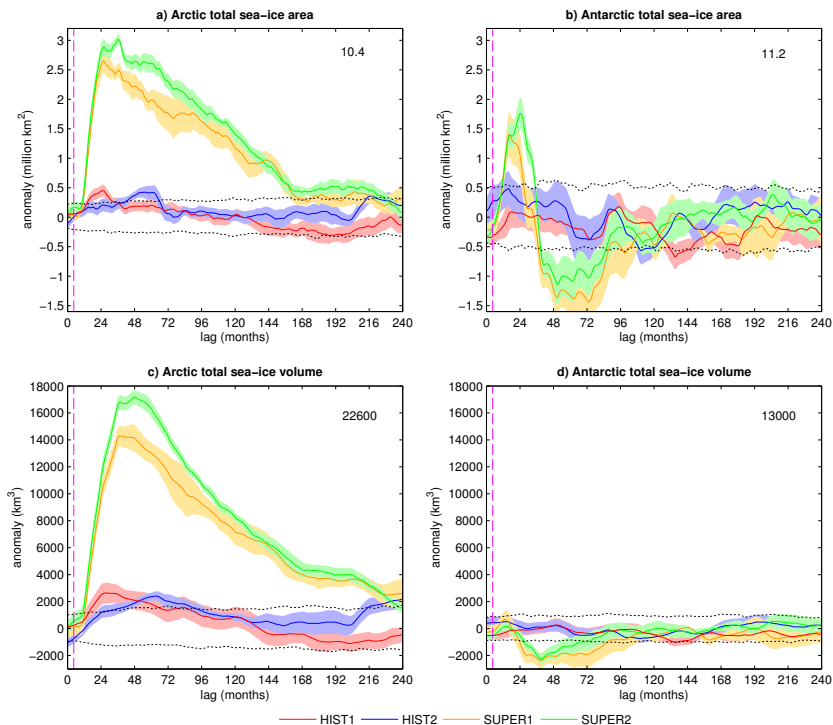


Fig. 3. Simulated post-eruption anomalies of Arctic (top panels) and Antarctic (bottom panels) total sea-ice area (top panels) and volume (bottom panels) for the two historical and the two “supervolcano” ensembles. Lines (shading): mean anomaly (standard error of the mean). Anomalies are smoothed with a 13 months centered moving average. Black dashed lines indicate the internal variability range ($n = 10$, see methods). The magenta vertical hatched line indicates the approximate start of the eruptions. Lag(0) corresponds to January of the eruption year. The number on top-right of each panel is the approximate pre-eruption climatology. The y axis has the same scale in (a) and (b), and in (c) and (d), highlighting the different magnitude of the hemispheric responses.

Inter-hemispheric asymmetry in the sea-ice response to volcanic forcing

D. Zanchettin et al.

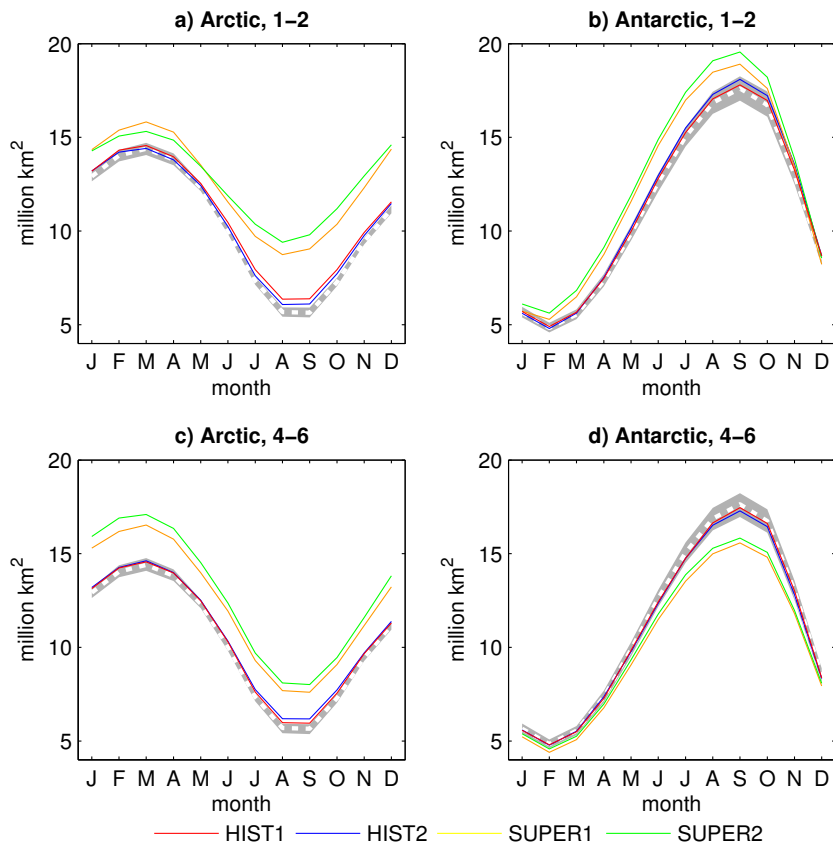


Fig. 4. Ensemble-mean simulated seasonal evolutions of hemispheric sea-ice area for integration years 1–2 (**a, b**) and 4–6 (**c, d**) for the two historical and the two “supervolcano” ensembles. Gray shading (hatched white line) represents the 98 % range (mean) for signal occurrence in the control run. Signal in the control run corresponds to the annual evolution averaged over three randomly chosen consecutive years, for a 10-member ensemble.

Inter-hemispheric
asymmetry in the
sea-ice response to
volcanic forcing

D. Zanchettin et al.

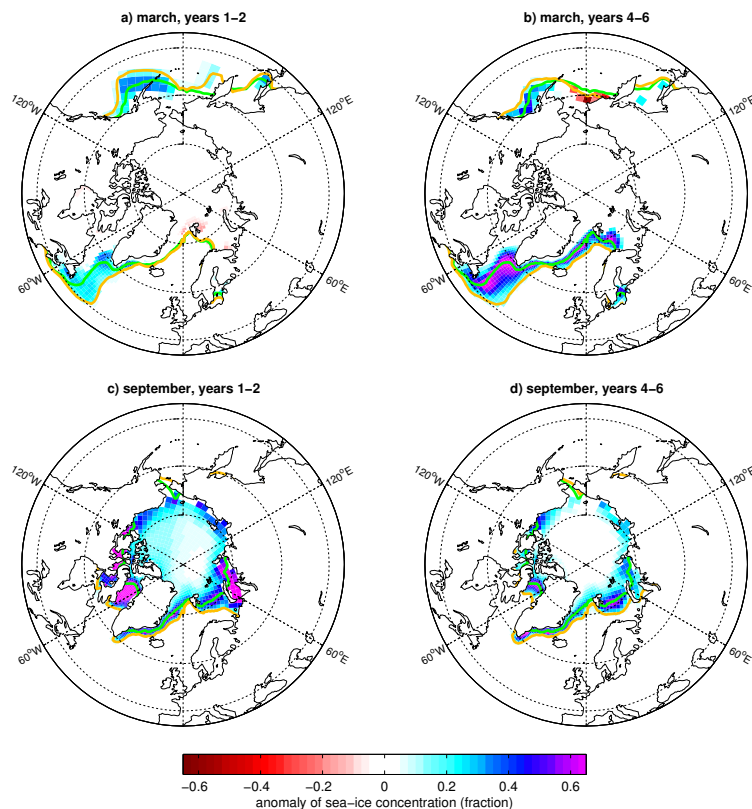


Fig. 5. Ensemble-mean simulated March (top panels) and September (bottom panels) Arctic sea-ice concentration anomalies for integration years 1–2 (**a**, **b**) and 4–6 (**c**, **d**) of the SUPER1 ensemble. Only grid points where the anomaly is significant at 95 % confidence ($n = 5$, see methods) are shown. The green and orange lines indicate, respectively, the pre-eruption average and post-eruption average sea-ice edge.

Inter-hemispheric
asymmetry in the
sea-ice response to
volcanic forcing

D. Zanchettin et al.

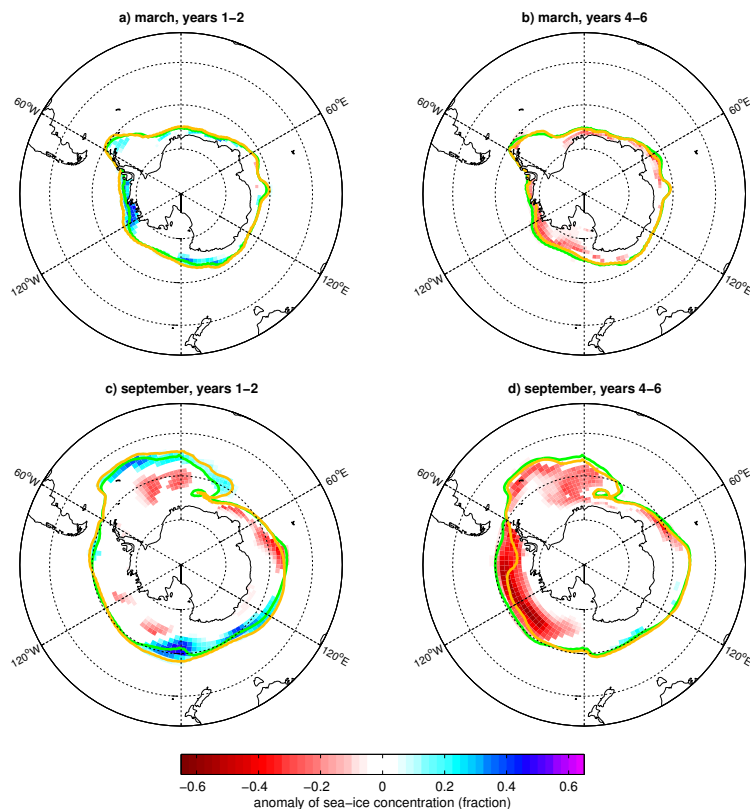


Fig. 6. Ensemble-mean simulated March (top panels) and September (bottom panels) Antarctic sea-ice concentration anomalies for integration years 1–2 (**a**, **b**) and 4–6 (**c**, **d**) of the SUPER1 ensemble. Only grid points where the anomaly is significant at 95% confidence ($n = 5$, see methods) are shown. The green and orange lines indicate, respectively, the pre-eruption average and post-eruption average sea-ice edge.

Inter-hemispheric asymmetry in the sea-ice response to volcanic forcing

D. Zanchettin et al.

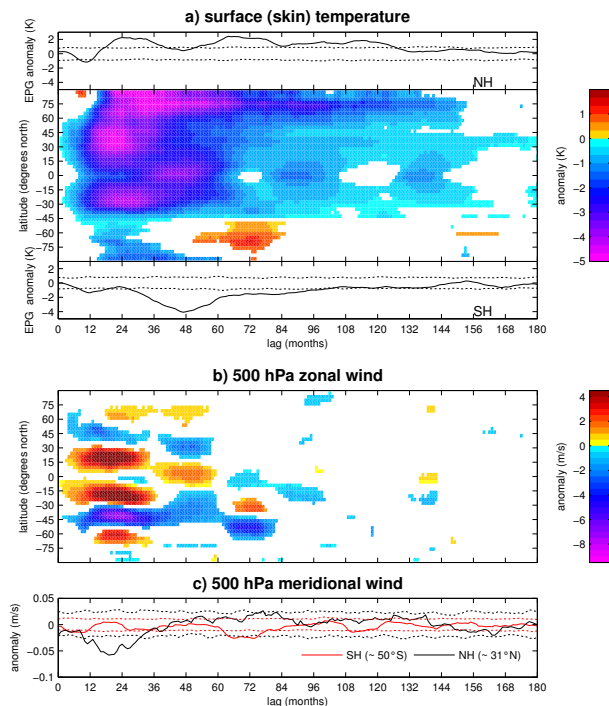


Fig. 7. Ensemble-mean post-eruption evolution of zonal-mean surface temperature **(a)**, zonal-mean 500 hPa meridional wind **(b)** and zonal wind **(c)** anomalies for the SUPER1 ensemble. Positive zonal and meridional winds are, respectively, eastward and northward. Filled contours in **(a, b)** Hovmoeller diagrams, only changes statistically significant at 99 % confidence are shown. Line plots in **(a)** anomalies of equator-to-pole gradient (EPG) for the Northern (top) and Southern (bottom) hemispheres. EPG is defined, for each hemisphere, as the difference between values at the grid latitude closest to the equator and the first grid latitude poleward of 70° . Dotted lines in **(a, c)** are 98 % confidence ranges. A 13 month running-average smoothing has been applied to all data.

[Title Page](#)
[Abstract](#)
[Introduction](#)
[Conclusions](#)
[References](#)
[Tables](#)
[Figures](#)
[Back](#)
[Close](#)
[Full Screen / Esc](#)
[Printer-friendly Version](#)
[Interactive Discussion](#)

Inter-hemispheric asymmetry in the sea-ice response to volcanic forcing

D. Zanchettin et al.

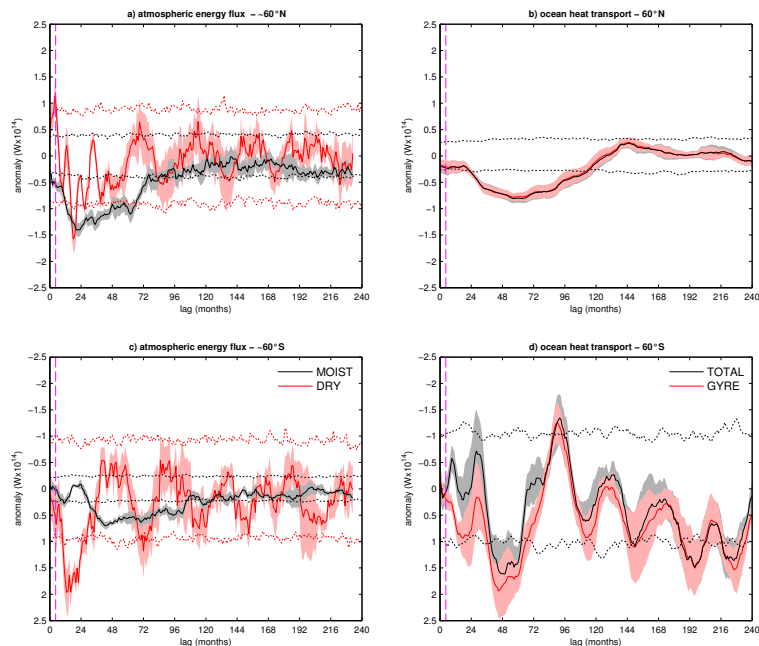


Fig. 8. Ensemble-mean simulated anomalies of zonally-integrated atmospheric energy transport at $\sim 60^\circ\text{N}$ (**a**) and $\sim 60^\circ\text{S}$ (**c**), and oceanic heat transport by advection at 60°N (**b**) and at 60°S (**d**) for the SUPER1 ensemble. Lines (shading): mean anomaly (standard error of the mean). Dashed lines indicate the internal variability range ($n = 5$, see methods). Internal variability ranges for the gyre component of ocean heat transport are not shown, since barely distinguishable from that of the total transport. The magenta vertical hatched line indicates the approximate start of the eruptions. Lag(0) corresponds to January of the eruption year. Anomalies are smoothed with a 13 months centered moving average. Positive values correspond to northward transport anomalies (y axis is inverted in **c** and **d**) to ease comparison of poleward transports in the two hemispheres.

Title Page

Abstract

Introduction

Conclusions

References

Tables

Figures

◀

▶

◀

▶

Back

Close

Full Screen / Esc

Printer-friendly Version

Interactive Discussion

Inter-hemispheric asymmetry in the sea-ice response to volcanic forcing

D. Zanchettin et al.

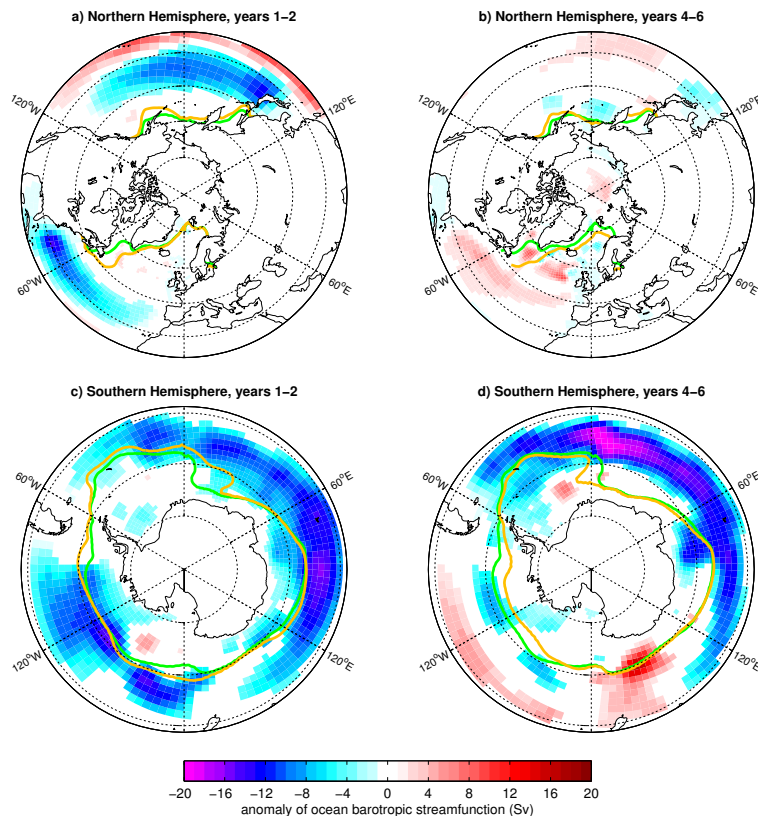


Fig. 9. Ensemble-mean simulated annual-average oceanic barotropic streamfunction for integration years 1–2 (**a, b**) and 4–6 (**c, d**) of the SUPER1 ensemble. Only changes statistically significant at 95 % confidence are shown. The green and orange lines indicate, respectively, the pre-eruption and post-eruption average winter (top panels: DJF, bottom panels: JJA) sea-ice edge.

Inter-hemispheric asymmetry in the sea-ice response to volcanic forcing

D. Zanchettin et al.

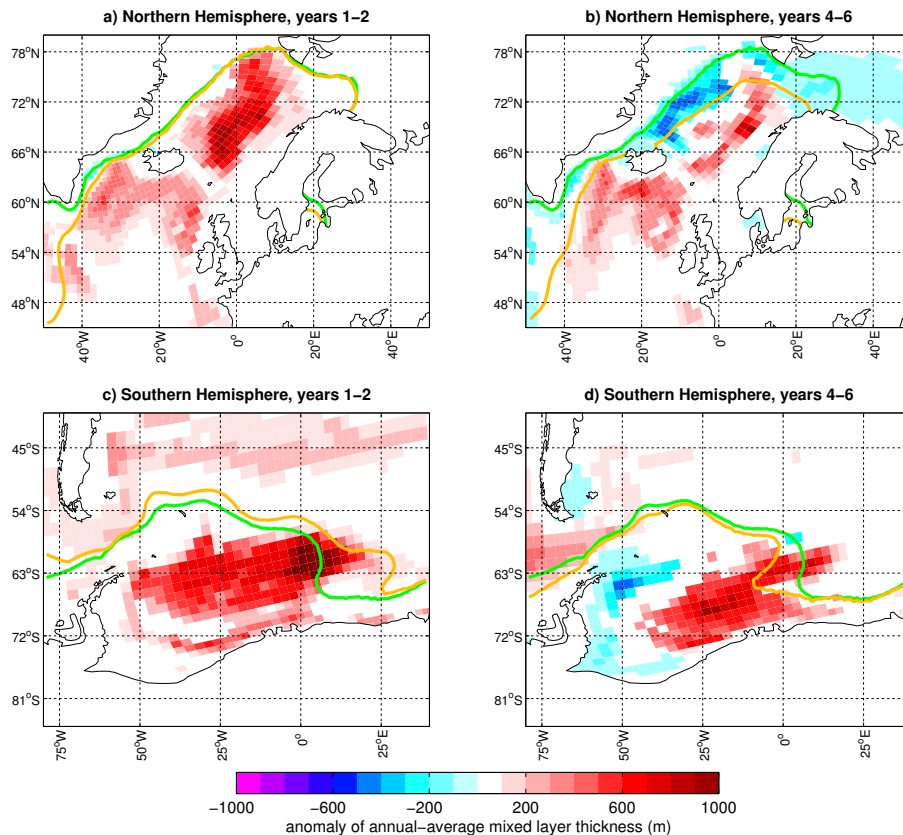


Fig. 10. Ensemble-mean simulated annual-average mixed layer thickness in two oceanic deep convection regions for integration years 1–2 (**a**, **b**) and 4–6 (**c**, **d**) of the SUPER1 ensemble. Only changes statistically significant at 95% confidence are shown. The green and orange lines indicate, respectively, the pre-eruption and post-eruption average winter (top panels: DJF, bottom panels: JJA) sea-ice edge.

Inter-hemispheric asymmetry in the sea-ice response to volcanic forcing

D. Zanchettin et al.

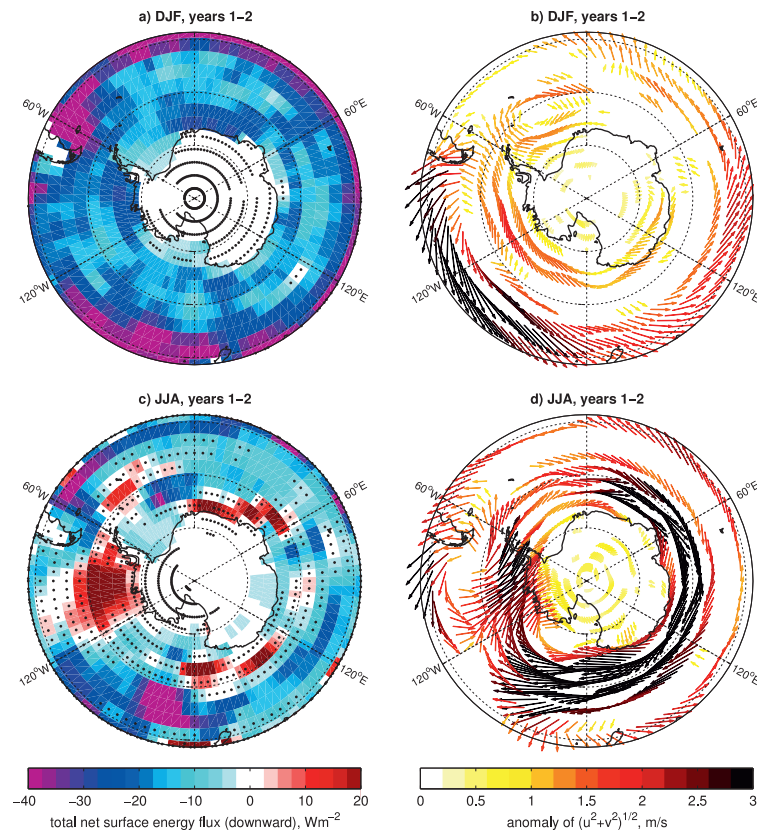


Fig. 11. Ensemble-mean simulated Southern Hemisphere summer (DJF, top) and winter (JJA, bottom) total net surface energy flux (latent and sensible heat, short- and long-wave radiation, **a, c**) and 10m wind anomalies (**b, d**) for integration years 1–2 of the SUPER1 ensemble. (**a, c**) Black dots indicate grid points where changes are non significant at the 95 % confidence level; (**b, d**) only changes statistically significant at 95 % confidence for at least one of the wind components are shown.

Inter-hemispheric asymmetry in the sea-ice response to volcanic forcing

D. Zanchettin et al.

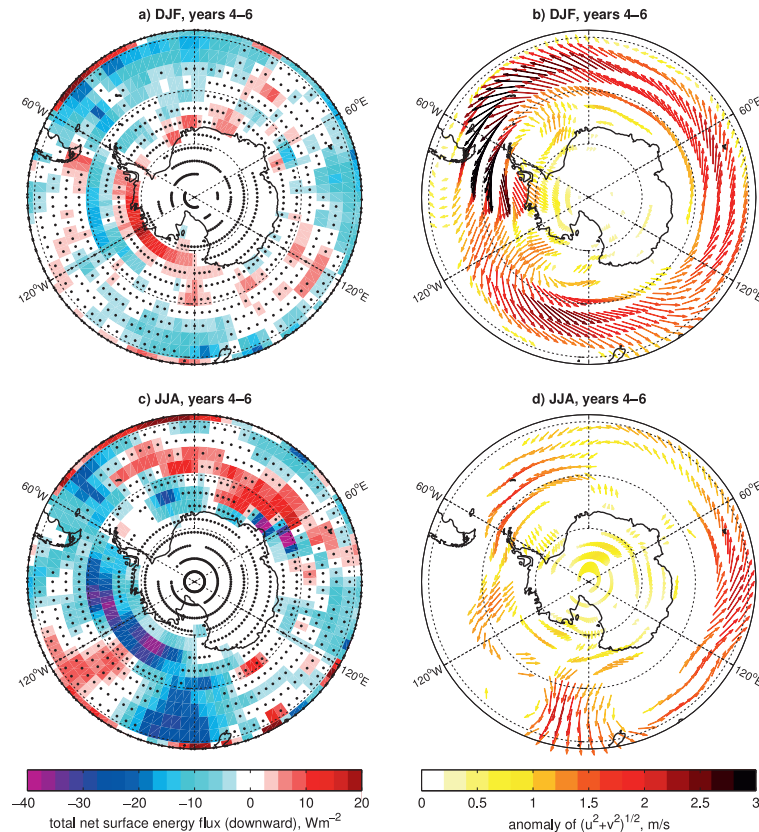


Fig. 12. Ensemble-mean simulated Southern Hemisphere summer (DJF, top) and winter (JJA, bottom) total net surface energy flux (latent and sensible heat, short- and long-wave radiation, **a, c**) and 10 m wind anomalies (**b, d**) for integration years 4–6 of the SUPER1 ensemble. (**a, c**) Black dots indicate grid points where changes are non significant at the 95 % confidence level; (**b, d**) only changes statistically significant at 95 % confidence for at least one of the wind components are shown.